Hybrid Laser Arc Welding of HY-80 Steel

The effects of process, power level, heat input, and preheat on the macrostructure and microstructure of hybrid welds in HY-80 steel were investigated

BY C. ROEPKE AND S. LIU

ABSTRACT

The macrostructure, microstructure, chemical composition, inclusions, and hardness of hybrid laser arc welds in HY-80 steel were evaluated. Experiments were conducted to compare hybrid laser arc welding (HLAW) to gas metal arc welding (GMAW) and laser beam welding (LBW). The effect of the laser power and arc power levels on weld morphology and the effects of heat input (controlled by travel speed) and preheat on microstructural control were studied. It was found that a minimum arc-to-laser power ratio exists to prevent laser-only penetration, and that the heat input of the hybrid process is dominated by the arc. It was shown that HLAW welds were microstructurally similar to GMAW welds with similar heat input but significantly improved from the LBW welds at similar laser powers. HLAW produced a suitable inclusion size distribution for the nucleation of acicular ferrite. Increasing the heat input in HLAW showed the expected trend of increasing the content of ferritic microstructures and reducing the weld metal hardness. Increasing preheat in HLAW increased the amount of acicular ferrite and reduced the hardness in both the fusion zone and heat-affected zone. This research work has shown that hybrid laser arc welding is a suitable process for welding high-strength, quenched-and-tempered grade steels using conventional control of heat inputs and preheats.

C. ROEPKE and S. LIU are with the Center for Welding, Joining, and Coatings Research, Colorado School of Mines, Golden, Colo.

Introduction

Hybrid laser arc welding (HLAW) is a combined process of gas metal arc welding (GMAW) and laser beam welding (LBW) incident on the same weld pool. It was first developed by Eboo and Steen in the late 1970s (Ref. 1). However, there has been limited research work on the process until recently because of the cost and availability of high-power welding lasers. Early research work has shown that the process can increase welding speeds with fewer surface defects and improved penetration (Refs. 1, 2). At lower laser powers (typically less than 1 kW) the hybrid process is dominated by the arc and the laser primarily is used for stabilization of the arc (Refs. 1, 3, 4). Typically for industrial applications, high laser powers (greater than 1 kW) are used. In addition to enhancements in welding speed and penetration over GMAW, the ability of HLAW to bridge gaps (LBW requires tight joint tolerances) has led to great industrial interest (Refs. 5–11). In this study, a high laser power is used, and the weld morphology is a combination of those of the laser and arc welds. Hybrid welding also has many new variables that are different from those of GMAW and LBW, e.g., laser-arc separation, angles, leading or following process, and power ratio. Much research work has been done on the effects of these parameters on penetration, gap bridging ability, welding

speed, energy and process efficiency, and joint geometries (Refs. 3, 5–11). However, only recently has there been research work on the characterization of the metallurgy and microstructure of the hybrid welds (Refs. 12–17). This paper focuses on the development of macrostructure and microstructure of hybrid laser arc welds.

High-yield (HY) steels are alloys within the quenched-and-tempered low-alloy steel family. They typically have 0.12 to 0.20 wt-% carbon with up to approximately 8 wt-% total alloy content. As such, they are hardenable and, when quenched, provide high strength in thick-section plates, and with tempering, good toughness. To improve the toughness of the HY grade steels, nickel is added as the main alloying element. There are three grades of HY steels with yield strengths of 80, 100, and 130 ksi (550, 690, and 900 MPa), and they are typically welded with an AWS E100S-1 type or similar welding wire. For HY-80 steel, austenitizing is done at 900°C followed by water quench and tempering at 650°C. The final steel microstructure is tempered martensite/bainite.

Autogenous welding of HY steels leads to a predominately untempered martensite weld metal microstructure because of the high carbon and alloy content and fast cooling rates. For these reasons, filler metals are generally required for the welding of HY steels. The filler metal can reduce the alloy content (hardenability) and carbon content (peak hardness) by dilution and provide new alloying elements (Mn, Al, and Ti) that will form oxide inclusions necessary for the nucleation of acicular ferrite, which is the desired microstructure for HY steel weldments. The acicular ferrite microstructure provides a good combination of strength and impact toughness. However, for the formation of an acicular ferrite microstructure a critical amount of filler metal must be added to the weld metal and the cooling rate cannot be too rapid (Refs. 18, 19).

The effect of inclusions on steel weld

KEYWORDS

Acicular Ferrite
Gas Metal Arc
HY-80 Steel
Hybrid Welding
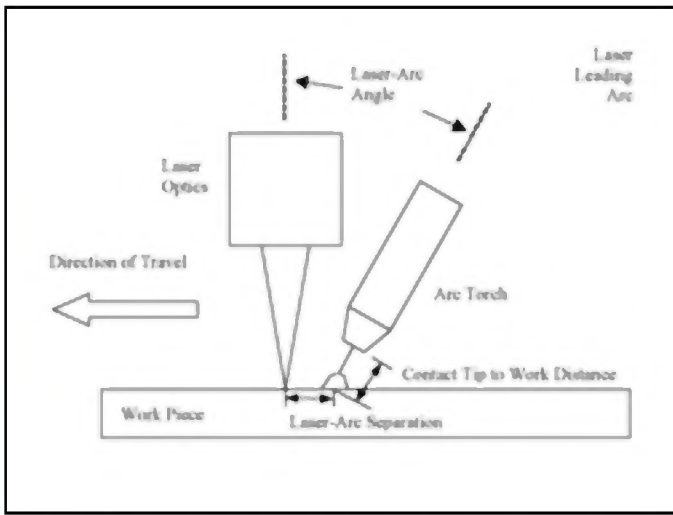Laser Beam Welding
Travel Speed

WELDING RESEARCH

Fig. 1 — Diagram of the experimental setup showing the processing constants.
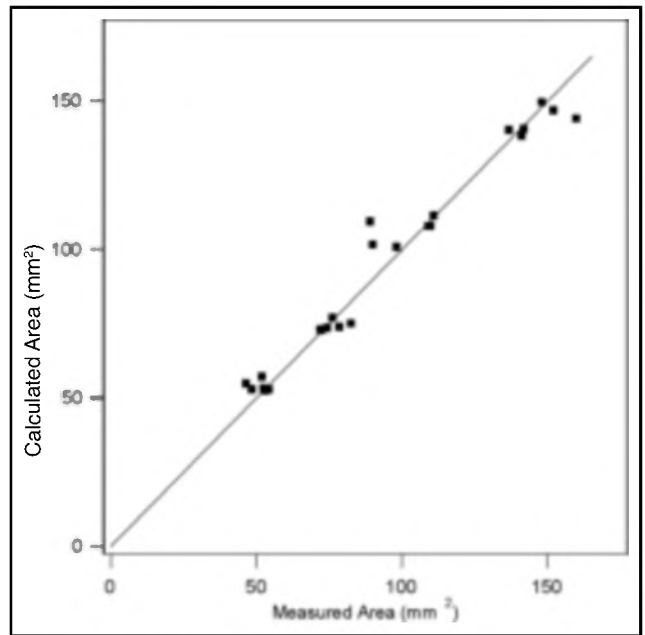

Fig. 2 — Fit of the measured weld areas to the areas calculated from the regression analysis, $R^2 = 0.967$.
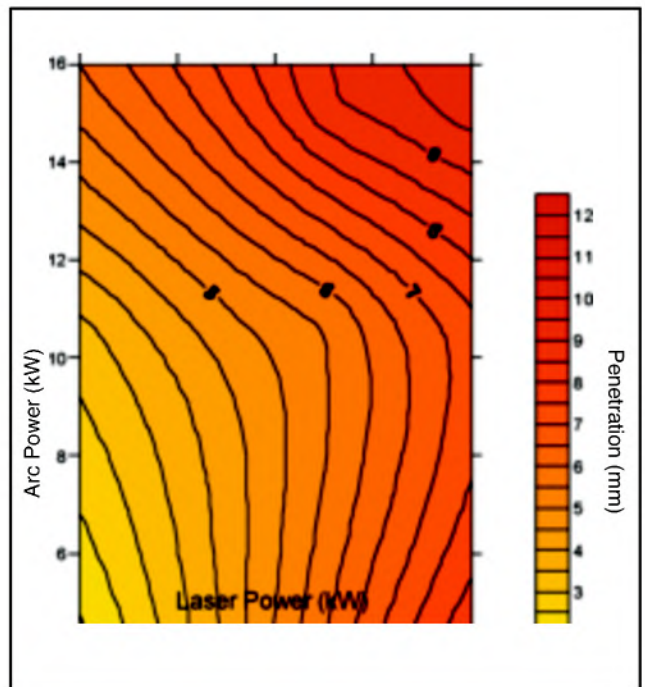

Fig. 3 — Map of weld penetration against laser power and arc power at 15 in./min travel speed.

metal microstructure is very important. As HY-80 steel possesses high hardenability, martensitic microstructures are readily found in HY-80 steel weldments that exhibit high strength, low ductility, and hydrogen cracking susceptibility (Refs. 18, 19). As was discussed in the previous paragraph, the presence of inclusions in a weldment will promote the nucleation of acicular ferrite (Refs. 20–26). The distribution of the inclusion sizes is critical for controlling the final microstructure. A low number of small inclusions with diameters smaller than the Zener diameter will allow austenite grain growth, consequently decreasing the amount of grain boundary ferrite formed in competition with acicular ferrite. There must also be a substantial amount of large intragranular inclusions of diameter between 0.4 and 0.6 µm to nucleate acicular ferrite (Refs. 20–22). The acicular ferrite content of the weld metal microstructure has been shown to increase with increasing inclusion size mode (Refs. 20, 21). Increasing the heat input of a weld increases the solidification time and consequently increases the average size of the inclusions resulting in an inclusion population more prone to nucleating acicular ferrite (Ref. 23). Specific alloying additions also contribute to the formation of oxide inclusions that will nucleate acicular ferrite.

Manganese is primary in importance for the formation of inclusions that will nucleate acicular ferrite, silicon and low levels of aluminum and titanium are also found in inclusions that nucleate acicular ferrite (Ref. 24). It is necessary that HLAW welds have a suitable inclusion population for the nucleation of acicular ferrite.

High-yield steels are typically welded with the application of preheat to prevent hydrogen-induced cracking. Because of the high hardenability of HY steels, due to their high alloy content, both the fusion zone (FZ) and heat afected zone (HAZ) of the weldment can develop hard micro-structures that are susceptible to hydrogen-induced cracking. The FZ microstructure can be readily controlled by alloy additions in the filler metal however, the HAZ microstructure must be controlled with preheat. In addition, low-hydrogen welding practices must be used when welding HY steels to reduce the amount of hydrogen initially present in the weldment. The application of too high a preheating temperature or a combination of high preheat and heat input can produce a very slow cooling rate in the HAZ resulting in a detrimental two-phase HAZ microstructure. On cooling from austenite, large amounts of ferrite are initially formed, rejecting carbon; then, because of the increased carbon content, the remaining austenite transforms into a brittle, high-carbon martensite. With an appropriate level of preheat for the heat input of the welding process, the cooling rate in the HAZ produces a martensite/bainite microstructure. The correct application of preheat when welding HY steels is important to prevent hydrogen-induced cracking and to produce an HAZ microstructure with similar properties to the base material.

Earlier work on HLAW HY-80 steel was not able to produce a weld metal microstructure of predominately acicular ferrite (Ref. 12). This was likely due to low manganese content in the weld metal because of greater dilution from the increased melting of the base metal (Ref. 12). Another study (Ref. 15), however, reported

that pipeline steels with higher levels of manganese were able to produce a weld metal microstructure with predominately acicular ferrite.

Research Objectives

The objectives of this research are as follows:
• To characterize the effects of laser and arc powers levels on the weld morphology,
• To develop a predominately acicular ferrite microstructure in the HLAW welds,
• To observe the effect of HLAW on the inclusion population of the welds, and
• To demonstrate control of the HLAW microstructure using different preheats and heat inputs.

Experimental Procedures

The laser arc hybrid welding system consisted of a continuous-wave 14-kW CO_2 laser with a F/# (ratio of raw beam diameter to focal length) of 5.2, a spot size of 1 mm and a constant voltage GMAW power source. The electrode was 1/16-in.-(1.6-mm) diameter ER100S-1 wire, fed using a conventional wire feeder and GMAW gun. The laser-electrode separation was held constant at 6 mm and the shielding gas used was 50%He-45%Ar-5%CO_2. Base material was 3/4-in.- (19-mm) thick HY-80 steel, cut into 4 × 8-in. (101 × 202-mm) coupons. Welding was done with the laser leading the arc. Contact tip-to-work distance and welding angles were all held constant throughout the experiment as shown in Fig. 1. All the constant processing parameters are shown in Table 1. Three separate experiments were done to examine the hybrid welding process. Welds were made comparing HLAW with GMAW and LBW. To examine the effect of heat input, laser power, arc current, and voltage were all kept constant while the travel speed was adjusted from 15 to 30 in./min (6.4 to 12.8 mm/s). Finally, the effect of preheat was studied with welds done at ambient temperature (80°F or 26.7°C) and at 140°F (60°C) and 250°F (121°C). In addition, two different laser powers (5 and 8 kW) and two different arc parameters (32 V with 200 in./min or 85 mm/s wire feed speed (WFS) and 35
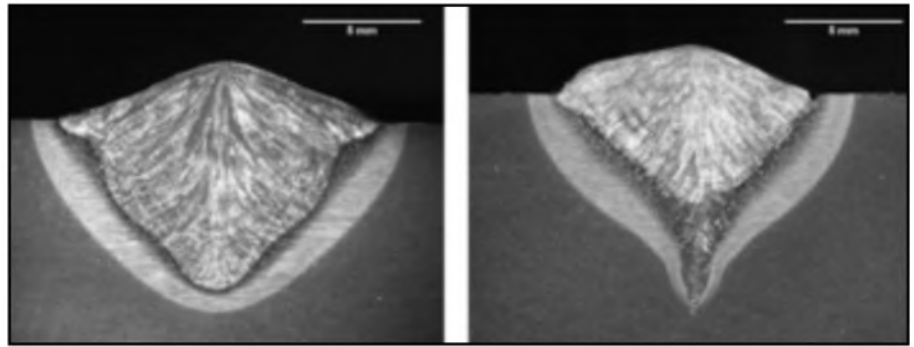
V with 300 in./min or 127 mm/s WFS) were used in heat input and preheat experiments to explore the parameter space for hybrid welding. Laser-only and arc-only tests were also done for comparison.

Samples from these weld specimens were taken and the weld surface was ground flush for chemical analysis using optical emission spectroscopy. In addition, the base metal chemical composition was also analyzed. A summary of the chemical compositions of these welds is shown in Table 2.

The welds were sectioned at least one inch from the weld start and weld stop and were ground and then polished down to 1- μm diamond suspension and etched with a 2% Nital solution for 10 s. Macrographs of the welds were taken using a stereomicroscope. The weld morphology was observed and characterizing dimensions such as width, penetration, and fusion zone area were measured.

The HLA welds that exhibited a uniform fusion zone with no laser-only penetration and the reference GMA and LB welds were repolished to 0.05 μm with alumina for microstructural characterization. Initially left

unetched, those welds were examined for inclusions using the light microscope as well as the scanning electron microscope (SEM). In the SEM, the backscatter electron detector was used to observe the presence of inclusions in the welds. Since most inclusions are oxides, they appear darker than the matrix material in the weld and could be readily distinguished from pits or any other topographical artifacts. Thirty backscatter images at 4000× magnification were taken and used for the analysis. An image analysis software, Image J, was used to locate and measure the area of each inclusion by adjusting the grey scale threshold. The minimum inclusion area measured was 0.005 μm². A statistical analysis of the inclusion populations for size distribution, number density, and volume fraction was performed. An inclusion size distribution histogram was made and the inclusion diameters were sorted into 0.05-μm bins. The histograms were fit using a gamma distribution function (Ref. 27) as shown below.

$$f(x) = A \cdot \frac{1}{\beta^\alpha \cdot \Gamma(\alpha)} \cdot x^{\alpha-1} \cdot e^{-x/\beta}$$

(1)

Fig. 4 — Left: pure hybrid weld with a uniform fusion zone; Right: hybrid weld with some laser-only penetration and nonuniform fusion zone.

Table 1 — HLAW Processing Constants

Welding position	Flat
Process orientation	Laser leading arc
Laser focus	At workpiece surface
GMAW polarity	DCEP-CW
Contact tip-to-work distance	0.75 in.
Laser-arc separation	6.0 mm
Laser-arc angle	15 deg
Shielding gas	50%He-45%Ar-5%CO_2
Shielding gas flow rate	150 ft³/h
Electrode	E100S-1, 1/16 in. diameter

Table 2 — Chemical Composition for the Welds of Interest

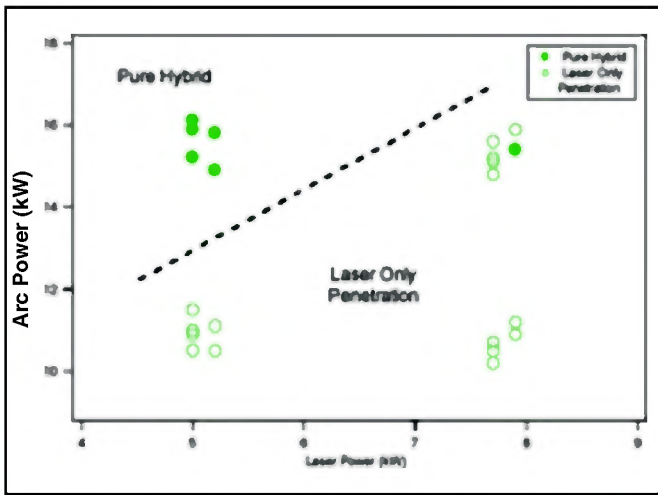| Weld No.	Process	C	Mn	Al	Si	Cr	Ni	Mo	V	Ti	Cu	CE	P_{CM}
3	HLAW	0.22	0.68	0.014	0.29	1.48	3.18	0.38	0.01	0.01	0.14	0.98	0.42
27	GMAW	0.20	0.96	0.016	0.35	0.98	2.69	0.37	0.01	0.02	0.11	0.87	0.38
25	LBW	0.21	0.29	0.012	0.22	1.53	2.65	0.27	0.01	0.01	0.11	0.84	0.38
4	HLAW	0.20	0.64	0.020	0.28	1.32	2.87	0.36	0.00	0.01	0.11	0.89	0.39
13	HLAW	0.20	0.68	0.019	0.29	1.22	2.82	0.37	0.01	0.01	0.11	0.87	0.38
16	HLAW	0.21	0.70	0.008	0.25	1.06	2.61	0.32	0.01	0.01	0.11	0.83	0.38

Fig. 5 — Parameter space map showing weld morphology (note the one pure hybrid weld in the upper right, this result is likely an outlier due to temporary decreased laser penetration at the location of the weld section).

Nital solution for 5 s, and photomicrographs were taken at 1000× magnification using the light microscope. Welds were examined for their microstructural constituents using the IIW guidelines for the classification of microstructures. Ten micrographs were taken from each weld and 100 points were counted on each micrograph for a total of 1000 point counts.

Finally, microhardness traverses were performed on the welds to relate microstructure to mechanical properties. A Vickers diamond indenter with a 500-g load was used. The hardness traverses were done at 0.100 in. (2.54 mm) below the base metal surface at 0.025-in. (0.635- mm) intervals with at least three measurements in the unaffected base metal on each side of the weld.

The inclusions were further characterized using the SEM, energy dispersive spectroscopy (EDS). The chemical composition of the inclusions was determined using the spot scan and mapping features of the EDS.

These welds were then etched with a 2%

Results and Discussion

The macrostructural analysis first examined the hybrid welds. Since weld area is directly proportional to heat input, a statistical analysis was performed using the *Minitab* software to examine how the welding parameters affected the weld morphology (bead shape, area, and penetration) and consequently the heat input. A broader experimental matrix (in addition to those described in Table 2) was performed for weld characterization and the data of these welds are given in Table 3. Initially in the analysis, the measured weld areas for the entire set of hybrid welds were set to be linearly related to preheat, travel speed (v), laser power (P_L), and arc power (P_A). A regression analysis was used to find the proportionality coefficients. The coefficient for preheat was orders of magnitude smaller than the other coefficients. Consequently, preheat was removed from the analysis because preheat would have a minimal effect on weld area. The coefficient for travel speed had a negative coefficient. Since the weld area is proportional to the energy input per unit length and not the power or the velocity directly, the power parameters were divided by the travel speed to obtain an en-

Table 3 — Process Variables and Weld Morphology Effects for All Welds

Weld No.	Process	Preheat (°F)	Travel Speed (in./min)	Laser Power (kW)	Arc Power (kW)	Penetration (mm)	Measured Area (mm²)	Pure Hybrid
2	HLAW	80	15	5.2	10.5	5.9	89.9	No
14	HLAW	140	15	5.0	11.5	5.4	89.1	No
15	HLAW	250	15	5.0	10.5	5.5	98.2	No
3	HLAW	80	15	5.2	14.9	8.9	141.0	Yes
13	HLAW	140	15	5.0	15.2	8.9	142.0	Yes
16	HLAW	250	15	5.0	15.2	8.9	137.0	Yes
7	HLAW	80	15	7.9	10.9	7.8	111.0	No
22	HLAW	140	15	7.7	10.5	6.7	110.0	No
21	HLAW	250	15	7.7	10.5	7.1	109.0	No
6	HLAW	80	15	7.9	15.4	11.2	148.0	Yes
18	HLAW	140	15	7.7	15.2	9.2	152.0	No
17	HLAW	250	15	7.7	14.8	8.7	160.0	No
1	HLAW	80	30	5.2	11.1	5.3	52.5	No
9	HLAW	140	30	5.0	10.9	5.0	53.3	No
10	HLAW	250	30	5.0	11.0	4.7	54.5	No
4	HLAW	80	30	5.2	15.8	7.2	72.3	Yes
12	HLAW	140	30	5.0	16.1	7.6	78.9	Yes
11	HLAW	250	30	5.0	15.9	7.4	72.1	Yes
8	HLAW	80	30	7.9	11.2	5.0	52.3	No
23	HLAW	140	30	7.7	10.2	7.9	48.5	No
20	HLAW	250	30	7.7	10.7	6.2	46.6	No
5	HLAW	80	30	7.9	15.9	7.8	76.5	No
24	HLAW	140	30	7.7	15.6	7.1	82.6	No
19	HLAW	250	30	7.7	15.1	6.9	74.4	No
26	GMAW	80	15	0.0	10.6	3.3	58.5	N/A
32	GMAW	140	15	0.0	10.6	2.9	55.9	N/A
29	GMAW	250	15	0.0	10.5	3.8	51.7	N/A
27	GMAW	80	15	0.0	15.5	6.7	101.0	N/A
33	GMAW	140	15	0.0	15.4	4.7	108.0	N/A
30	GMAW	250	15	0.0	15.4	5.9	107.0	N/A
25	LBW	80	15	7.7	0.0	8.9	44.7	N/A
31	LBW	140	15	7.7	0.0	13.4	54.0	N/A
28	LBW	250	15	7.7	0.0	9.5	49.1	N/A

WELDING RESEARCH

ergy per unit length parameter. Because the energy transfer efficiency of the individual energy sources in the hybrid process is not known, no efficiency term was applied to either the laser or the arc power. By not applying an efficiency term and then taking the ratio of the coefficients on the laser and arc energy terms, the relative contribution of each energy source to the melting can be estimated. The fitting equation for weld area (A) is shown below.

$$A = k_L \frac{P_L}{\nu} + k_A \frac{P_A}{\nu} \qquad (2)$$

Using a regression analysis the following fit coefficients were determined.

$k_L = 15.8 \qquad k_A = 53.5$

Using this equation and fit coefficients the measured area was accurately calculated over the range of the data — Fig. 2. While the fit coefficients by themselves have little physical significance, their ratio provides an estimate of the relative contribution of the two power sources to melting. The ratio between the arc energy coefficient and the laser power coefficient is 3.4, indicating that arc power contributed 3.4 times more to the weld area than the laser power. Since heat input is proportional to the weld area, it can be concluded that the arc dominates the heat input in the hybrid process. The heat transfer and melting efficiency of the hybrid welding process was not determined; however, other research work (Ref. 28) has shown that the interaction of the laser and arc does not change the heat transfer efficiency but does improve the melting efficiency.

In the macrostructural examination, it was observed that at all arc power levels, the addition of the laser immediately improved weld penetration, and continued to
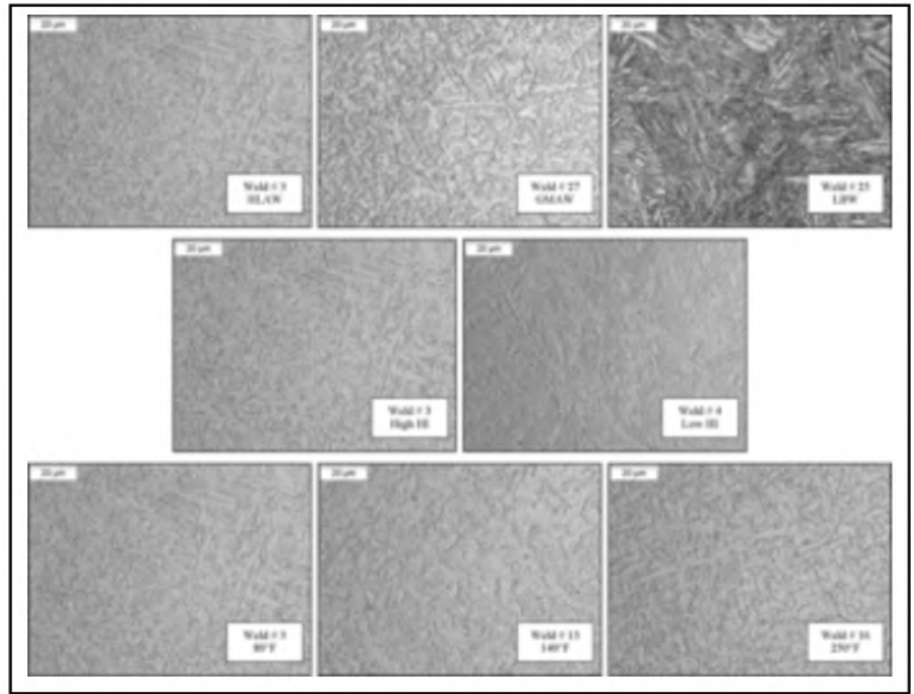

Fig. 6 — Light micrographs of the welds of interest. First row shows the process comparison, second row shows the heat input comparison, and third row shows the preheat comparison.

increase penetration as laser power was increased. At low laser power levels, up to about 5 kW, the addition of arc power also increased weld penetration. Above 5-kW laser power, however, the addition of the arc to the laser initially decreased penetration, likely because of both the destabilization of the keyhole by the arc and the increased absorption of the laser by the arc plasma. Continuing to increase the arc power to levels above 12 to 14 kW then increased the penetration. This effect is shown in Fig. 3. Weld width increased with both the laser power and arc power. The depth-to-width ratio followed a similar trend to penetration.

When examining the hybrid welds two distinct morphologies were seen — Fig. 4. Some of the welds had a two-section fusion zone: a GMAW-like upper section and some laser-only penetration below as shown in the right-hand-side macrograph. The upper section of the weld profile can be easily described by a semihemispherical geometry. The root part of the weld shows a finger-like penetration clearly illustrating the laser keyhole effect. This morphology has been observed before by
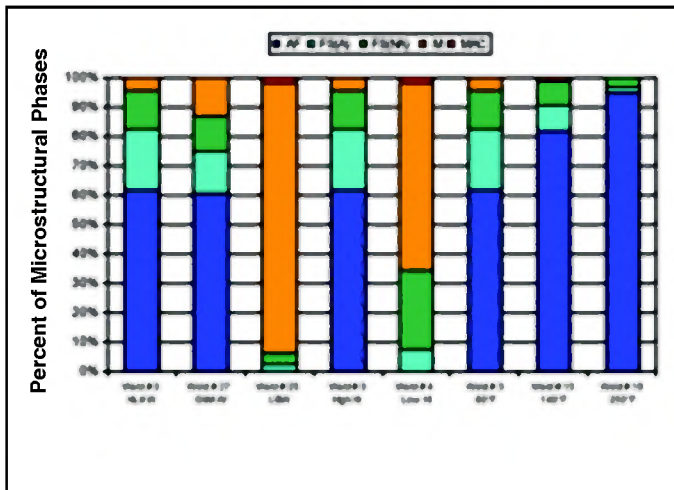

Fig. 7 — Weld metal microstructures of the welds of interest. First three bars show the process comparison, middle two bars show the heat input comparison, and last three bars show the preheat comparison.
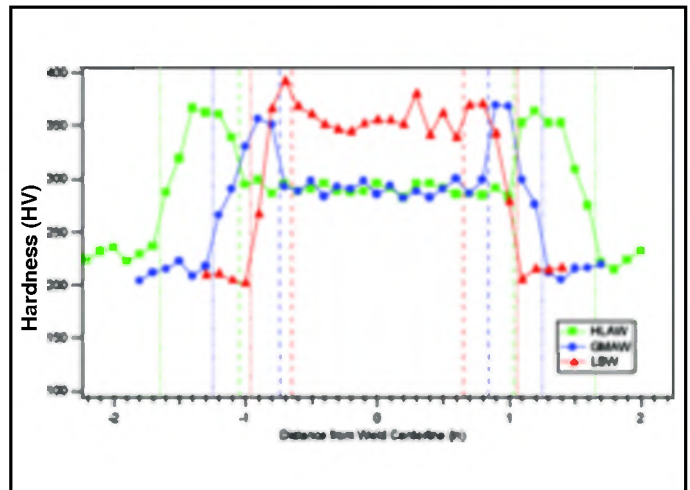

Fig. 8 — Weld hardness traverses comparing processes. The coarse dotted line shows the location of the weld interface and the fine dotted line shows the location of the HAZ–unaffected base metal boundary.
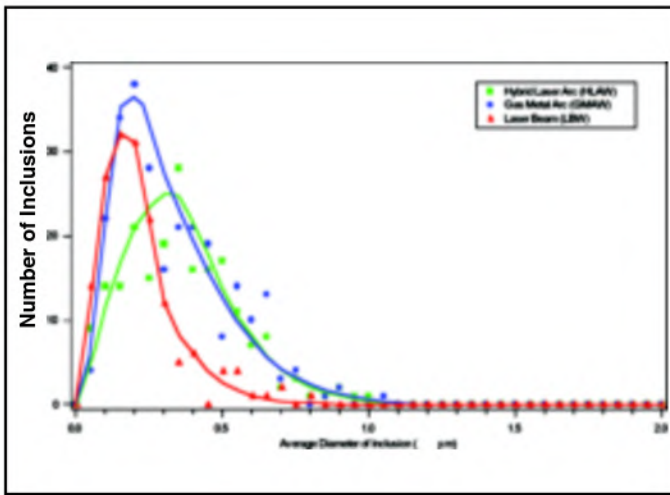
Fig. 9 — Weld metal inclusion size distributions comparing processes.
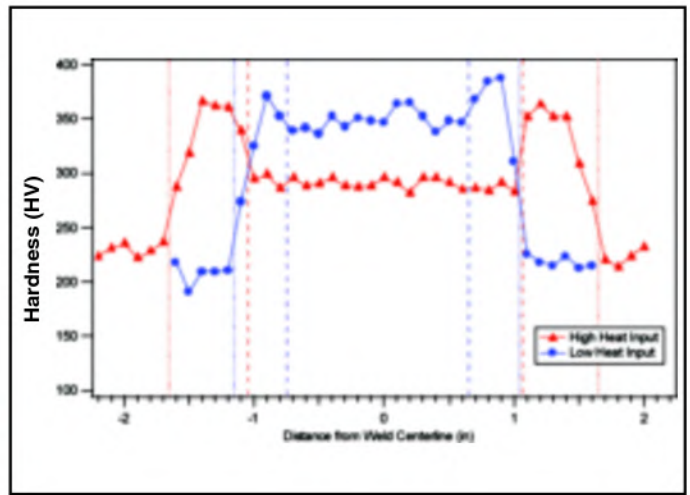

Fig. 10 — Weld hardness traverses comparing heat input. The coarse dotted line shows the location of the weld interface, and the fine dotted line shows the location of the HAZ-unaffected base metal boundary.

previous researchers at an arc-to-laser power ratio of 1.2 (Refs. 13, 29). This work also showed a more ferritic microstructure in the upper GMAW-dominated zone and more martensite in the lower LBW-dominated zone. They also observed reduced mixing of the filler metal in the laser-only zone. While the mechanism for the formation of this morphology has not been studied in detail, it is possible that there is incomplete mixing of the molten pool from the GMAW in the back to the front and down the LBW keyhole. It is also conceivable that the bottom of the LBW keyhole is at least partially solidified and not remelted by the GMAW. The other group of welds as shown in the

right-hand-side macrograph in Fig. 4 had a uniform fusion zone with no GMAW-like or LBW-like section. Named as pure hybrid in this work, this macrostructure is the generally desired morphology because of its uniformity in chemical composition and microstructure. This morphology has been reported numerous times in the literature (Refs. 5–12).

These two distinct morphologies were mapped on a laser power vs. arc power parameter space — Fig. 5. It was observed that the power ratio of arc power-to-laser power determined whether the weld was a pure hybrid weld or had some laser-only penetration. A high ratio of arc-to-laser power produced pure hybrid welds, while

low ratios of arc-to-laser power produced welds with some laser-only penetration. This effect was observed to be independent of both travel speed and preheat. This power ratio provides the upper limit on laser power for the hybrid process. For the welding parameters tested and the 6-mm laser-arc separation, the boundary between the two morphologies was between an arc-to-laser power of 2 and 3. This boundary is likely dependent on the laser-arc separation; decreasing the laser-arc separation should result in more pure hybrid welds and lower the arc-to-laser power ratio limit (Ref. 29). It should be noted that when mapping the pure hybrid weld morphology, one of the pure hybrid

Table 4 — The effects of Process, Heat Input, and Preheat on the Cooling Rate, Acicular Ferrite Content, and Average Weld Metal Hardness for the Welds of Interest

Weld No.	Process	Preheat (°F)	Heat Input (kJ/mm)	Δt_{8-5} (s)	Acicular Ferrite Content (Vol-%)	Average Weld Metal Hardness (HV)
3	HLAW	80	1.9	6.0	62	290.3
27	GMAW	80	1.8	5.8	61	290.6
25	LBW	80	0.6	1.9	0	367.4
4	HLAW	80	1.0	3.1	0	347.9
13	HLAW	140	1.9	6.8	82	254.2
16	HLAW	250	1.9	8.6	95	240.0

Table 5 — Inclusion Parameters for the Welds of Interest

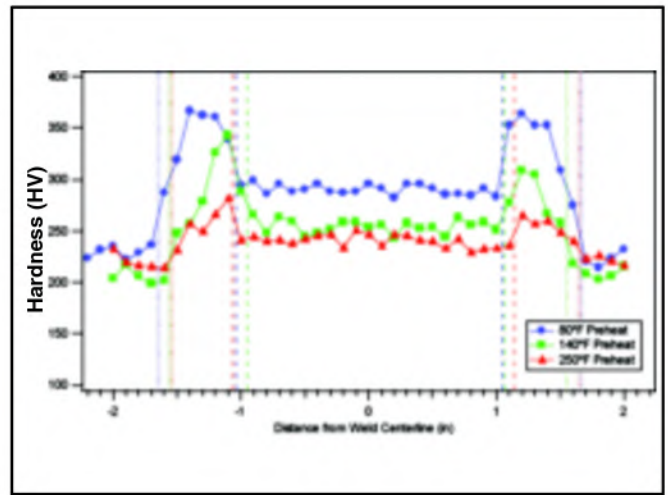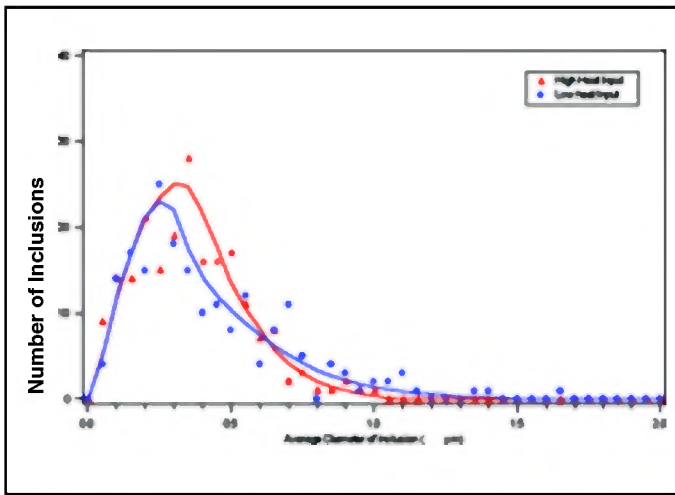| Weld No.	Process	Number Fraction (No./mm²)	Inclusion Volume Fraction (vol-%)	Inclusion Ratio Large to Small	Inclusion Diameter Mode (μm)	Median Inclusion Diameter (μm)
3	HLAW	6474	0.071	4.6	0.35	0.367
27	GMAW	7642	0.073	3.3	0.20	0.311
25	LBW	5066	0.021	1.2	0.15	0.221
4	HLAW	5747	0.084	4.6	0.25	0.371
13	HLAW	5786	0.070	4.8	0.20	0.355
16	HLAW	6724	0.072	4.4	0.25	0.337

Fig. 11 — Weld metal inclusion size distributions comparing heat input.

Fig. 12 — Weld hardness traverses comparing preheat. The coarse dotted line shows the location of the weld interface, and the fine dotted line shows the location of the HAZ-unaffected base metal boundary.

welds fell in the laser-only penetration region — Fig. 5. This outlier result is likely due to laser beam "spiking," where the penetration of a laser beam weld can vary by several millimeters because of instability of the keyhole and laser energy absorption. It is likely that this outlier weld was sectioned at a location where the laser penetration was temporarily lower than normal because of keyhole instability; consequently, the weld section had the pure hybrid morphology.

Microstructural characterization was performed on welds described in Table 2 that exhibited only the pure hybrid morphology, i.e., from the high arc power and low laser power group. The characterization also included the reference GMA and LB welds to examine the effects of process, heat input, and preheat. All the HLA welds of interest had the same laser (~5 kW) and arc (~15 kW) parameters. The GMA weld had the same arc parameters as the HLAW but with no laser power, but the LB weld had a higher power level (~8 kW) than the HLAW laser power in order to provide additional heat input. Changes in heat input of the HLA welds were made by changing the travel speed. Welds 3 (HLAW), 27 (GMAW), and 25 (LBW) were used to compare the three processes. Welds 3 (high heat input) and 4 (low heat input) were used to examine the influence of heat input, and Welds 3 (80°F preheat), 13 (140°F preheat), and 16 (250°F preheat) were used to study the effect of preheat. The identification of these welds and related cooling rate, microstructures, and hardness information are given in Table 4.

Through light microscopy, a wide range of microstructures was observed in these welds of interest. The micrographs from these welds are shown in Fig. 6. As mentioned earlier, the IIW guidelines for the identification of weld metal microstructures were used to quantify the phases present in the microstructures. The microstructural makeup in volume-percent of each of these welds is shown in Fig. 7

The first microstructural comparison made was the effect of the processes using Welds 3 (HLAW), 27 (GMAW), and 25 (LBW). As Fig. 6 shows, the HLA weld metal microstructure was similar to the GMA weld metal microstructure but different from that found in the LB weld. Both the HLA and GMA welds exhibited predominant (more than 60 vol-%) acicular ferrite microstructure. The remainder is mostly ferrite with secondary phases, approximately 20 to 30 vol-% — Fig. 7. However, the LB weld metal microstructure did not contain acicular ferrite. Only a small amount of ferrite with secondary phases, less than 10 vol-%, was observed. The majority of the microstructure was martensite — Fig. 7.

The resultant weld metal hardness for the GMA and HLA welds was similar, approximately 290HV. The LB weld metal exhibited much higher hardness, approximately 370HV — Table 4. The hardness traverses also show this effect — Fig. 8. The LB weld had high weld metal hardness, nearly equivalent to its HAZ hardness. The HLA weld metal hardness and
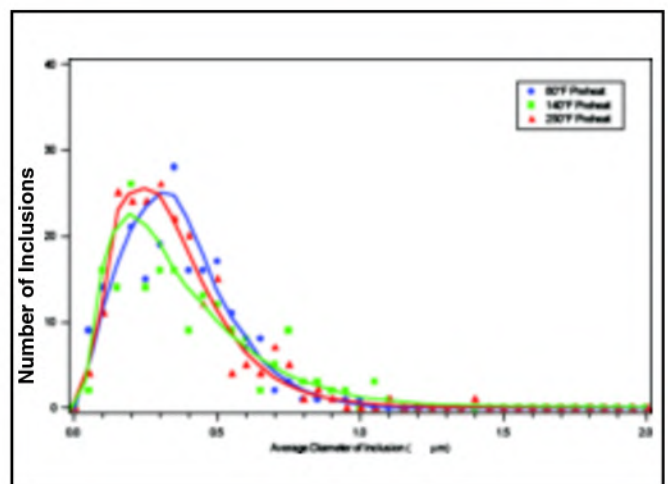

Fig. 13 — Weld metal inclusion size distributions comparing preheat.

GMA weld metal hardness are again nearly identical. Their peak hardness in the HAZ is also similar. The LB weld had the narrowest bead at approximately 0.3 in. The HLA weld, on the other hand, had the widest bead at almost 0.3 in. It also had a wider HAZ than the other two welds.

In the inclusion analysis, three different size distributions were observed for the three welds examined, as shown in Fig. 9. The LB weld inclusion size distribution was skewed to the left, with a large population of smaller inclusions but very few inclusions above 0.5 μm diameter. The inclusion size mode is around 0.15 μm. The GMA weld inclusion size distribution was also skewed to the left, i.e., with a large number of small inclusions, but it had a greater number of large inclusions. The inclusion size mode for the GMA weld is 0.2 μm. Comparatively, the LB weld was cleaner than the GMA weld.

The HLA weld inclusion size distribution exhibited a more normal behavior, with the size mode located at 0.35 μm. Its large inclusion size distribution was similar to the GMA weld, but the HLA weld had a smaller number fraction because of much fewer small inclusions. Note that both the HLW weld and the GMA weld have an acicular ferrite microstructure. The smaller number fraction of inclusions in the HLA weld will result in improved impact properties than for the GMA weld. In order to characterize the tendency of a given inclusion size distribution to nucleate acicular ferrite, the number ratio of large-to-small inclusions was calculated and the results are summarized in Table 5. The division between small and large inclusions was assumed to be 0.2 μm since inclusions of at least 0.2 μm in diameter have been observed to be necessary to nucleate acicular ferrite (Refs. 20–22). When this ratio of the number of large-to-small inclusions is large, the inclusion size distribution should have a greater tendency to nucleate acicular ferrite. The HLA weld has the highest ratio of large-to-small inclusions (4.6). The ratio for GMAW was moderately high (3.3) and the LBW the lowest (1.2). The inclusion size distribution of both HLAW and GMAW should readily nucleate acicular ferrite.

The cause of the differences in the inclusion size distributions of these welds is likely the weld metal chemical composition, specifically the manganese content (Table 2). Using the EDS capabilities of the SEM, the inclusions were determined to be predominately manganese-containing oxides. With low manganese in the HY-80 steel base metal, the autogenous LBW weld would have little manganese available to produce inclusions capable of nucleating acicular ferrite. On the other hand, the filler metal used in HLAW and GMAW is rich in manganese. These welds would be expected to exhibit higher levels of manganese and consequently a larger number of inclusions. The HLA weld had a larger fusion zone than the GMA weld because of the additional laser energy. The wire feed rates for both processes were the same. As a result, the HLA weld had greater dilution of the filler metal, and therefore lower manganese content, and smaller number of inclusions than the GMA weld.

The difference in weld metal microstructure between the three processes is also due to the different cooling rates experienced by the welds. Since the LB weld had a much lower heat input than both the HLA and GMA welds, its cooling rate expressed as Δt_{8-5} was expected to be much faster. This speculation was substantiated by calculations that the Δt_{8-5} of the LBW was 1.9 s, much shorter than the HLA weld, $\Delta t_{8-5} = 6.0$ s, or the GMA

weld, $\Delta t_{8-5} = 5.8$ s. These cooling rate calculations were made using the Rosenthal solution. The cooling path experienced by the LB weld, due to fast cooling, completely misses the ferrite nose on the CCT diagram. Even with proper size distribution of inclusions it is unlikely that the LB weld would produce a ferritic microstructure. The additional heat input of the arc, which slows the cooling rate and makes nucleation of ferritic phases possible, is a key advantage of HLAW over LBW.

The next microstructural comparison made was to investigate the effect of heat input in HLAW, using Welds 3 (high heat input) and 4 (low heat input). As mentioned earlier in the procedures section, the heat input was controlled by altering only the travel speed and not the laser or arc parameters. This practice was chosen to isolate the observations to only the effect of heat input and not the other process variables. Figure 6 shows the great differences observed in the two weld metal microstructures. The high heat input weld had a predominately acicular ferrite microstructure, more than 60 vol-%, with the remainder mostly ferrite with secondary phases, more than 30 vol-% — Fig. 7. However, the low heat input weld had no acicular ferrite and only a moderate amount of ferrite with secondary phases, approximately 35 vol-%. The rest of the microstructure was martensite — Fig. 7.

Weld metal hardness measurements showed low values for the high heat input weld, 290 HV, and high for the low heat input weld, 350 HV (Table 4). Figure 10 shows the hardness traverses for these welds. Increasing the heat input increases the size of the HAZ but decreases the weld metal hardness. While the low heat input weld had high hardness in the weld metal, it was slightly softer than the peak hardness found in the HAZ.

The inclusion size distributions for the two different heat input welds were similar — Fig. 11. However, the high heat input weld inclusion size distribution was shifted to the right (larger diameters), likely due to a longer time above melting than the low heat input weld allowing more time for the growth of the inclusions. Both inclusion size distributions have the same high ratio of large-to-small inclusions and inclusion modes and medians above 0.2 μm (Table 5). More specifically, the inclusion size mode of the higher heat input weld was 0.35 μm, instead of 0.25 μm for the lower heat input weld. Consequently, both welds have the necessary inclusions to nucleate acicular ferrite. These similarities in inclusion size distribution are expected because the two welds have nearly identical chemical compositions (Table 2), particularly the manganese content that is necessary for the formation of inclusions. However, the microstructures of the two

welds are very different and, therefore, inclusion size distribution cannot be solely responsible for the microstructure. The cooling rate has an important effect of controlling the microstructure. Because the cooling rate was high in the low heat input weld, $\Delta t_{8-5} = 3.1$ s, weld metal microstructure shows that the transformation to ferritic phases was almost entirely missed. Increasing heat input lowered the cooling rate and promoted the formation of acicular ferrite. It can be safely concluded that HLAW responds to heat input changes just as conventional GMAW.

The final microstructural comparison made was to examine the effect of preheat in HLAW. Welds 3 (80°F preheat), 13 (140°F preheat), and 16 (250°F preheat) were used. As Fig. 6 shows, all three welds had similar weld metal microstructures of predominately acicular ferrite. Increasing the preheating temperature increased the content of acicular ferrite and lowered the content of ferrite with secondary phases and martensite — Fig. 7. The weld at the lowest preheat, 80°F, was 62 vol-% acicular ferrite, and the weld at the highest preheat, 250°F, was 95 vol-% acicular ferrite.

The weld metal hardness at the lowest preheat of 80°F was 290 HV, but increasing the preheat to only 140°F lowered the weld metal hardness to 250 HV. Further increasing the preheat to 250°F continued to lower the weld metal hardness (240 HV), but not as dramatically (Table 4). Figure 12 shows the hardness traverses for these welds. Increasing preheat reduces the weld metal hardness but more importantly lowers the peak hardness in the HAZ. Note that preheat is the only process variable that significantly lowered the peak hardness in the HAZ. This is important because preheat can prevent the formation of a hard microstructure in the HAZ that makes HY-80 steel susceptible to hydrogen-induced cracking.

The inclusion size distributions of the welds at the three different preheat levels are nearly identical as shown in Fig. 13. They have similar inclusion volume fractions, median inclusion diameter, and ratio of larger-to-small inclusions (Table 5). This is again due to the uniformity in chemical composition specifically manganese (Table 2) and nearly identical time above melting (preheat has little effect on peak temperature or time above melting temperature). All of the welds had a suitable distribution of inclusions to nucleate acicular ferrite, and changing preheat had little effect on the inclusion size distribution. However, there were differences in the microstructures caused by the changes in cooling rate because of preheat. The 80°F preheat had a $\Delta t_{8-5} = 6.0$ s and the 250°F preheat had a $\Delta t_{8-5} = 8.6$ s. This change in cooling rate was significant enough to promote the nucleation of aci-

cular ferrite at slower cooling rates. HLAW responds to preheat control just as conventional GMAW.

Conclusions

The major conclusions from this research on hybrid laser arc welding of HY-80 steel are summarized below.

1) The addition of laser power to GMAW immediately begins to increase penetration; however, the addition of arc power to LBW initially decreases penetration, but then improves penetration as arc power is increased.

2) Arc power was found to dominate the melting (fusion zone area) and consequently the heat input over the laser power by a factor of 3.4 in the hybrid process. Substantially more energy was being transferred by the arc than the laser.

3) There is an upper limit to the laser power in HLAW defined by a ratio of arc-to-laser power that produces a pure hybrid weld with no laser-only characteristic. For the parameters tested, particularly the 6 mm of laser-arc separation, arc-to-laser power ratios greater than at least two are required for a pure hybrid weldment with no laser-only penetration.

4) The HLAW had suitable inclusion size distribution for the nucleation of acicular ferrite. Similar to the GMA weld, HLA welds showed a significant increase in acicular ferrite content and lower hardness than LB welds. This behavior is a combined result of the slower cooling rate and the improved inclusion size distribution of the hybrid weld.

5) Even though increasing heat input of HLAW by controlling travel speed had only a minor effect on the inclusion population, it greatly increased the amount of acicular ferrite in the weld metal, and lowered the weld metal hardness.

6) Increasing the preheat of HLAW had little effect on the inclusion population, but it increased the acicular ferrite content of the weld metal, and lowered the hardness of both the fusion zone and HAZ.

References

1. Steen, W. M., and Eboo, M. 1979. Arc augmented laser welding. *Metal Construction* 11 (7): 332–335.
2. Matsuda, J., et al. 1988. TIG or MIG arc augmentented laser welding of thick mild steel plate. *Joining and Materials* 1 (1): 38–41.
3. Bagger, C., and Olsen, F. O. 2005. Review of laser hybrid welding. *Journal of Laser Appli-*cations 17 (1): 2–14.
4. Tusek, J., and Suban, M. 1999. Hybrid welding with arc and laser beam. *Science and Technology of Welding and Joining* 4 (5): 308–311.
5. Dilthey, U., and Wieschemann, A. 2000. Prospects by combining and coupling laser beam and arc welding processes. *Welding in the World* 44 (3): 37–46.
6. Dilthey, U., et al. 1999. Technical and economical advantages synergies in laser arc hybrid welding. *Welding in the World* 43 (Supplementary Issue): 141–152.
7. Wieschemann, A., et al. 2001. Development of laser-GMA hybrid- and hydra welding processes for shipbuilding. *Welding in the World* 45 (7/8): 10–15.
8. Thomy, C., et al. 2005. Application of high-power fibre lasers in laser and laser-MIG welding of steel and aluminium. *Welding in the World* 49 (Special Issue): 88–98.
9. Shi, G., and Hilton, P. 2005. A comparison of the gap bridging capability of CO_2 laser and hybrid CO_2 laser Mag welding on 8-mm thickness C-Mn steel plate. *Welding in the World* 49 (Special Issue): 75–87.
10. Staufer, H. 2005. High productivity by using laser-GMAW- and laser-tandem-hybrid-process for thick plates. *Welding in the World* 49 (Special Issue): 66–74.
11. Jokinen, T. 2005. Novel ways of using Nd:YAG laser for welding thick section austenitic stainless steel. *Welding in the World* 49 (9/10): 11–18.
12. Hyatt, C. V., et al. 2001. Laser-assisted gas metal arc welding of 25-mm-thick HY-80 plate. *Welding Journal* 80 (7): 163-s to 172-s.
13. Liu, Z., et al. 2006. Microstructure and mechanical properties of CO_2 laser-MAG hybrid weld of high strength steel. *Quarterly Journal of the Japan Welding Society* 24 (4): 18–23.
14. Metzbower, E. A., et al. 2003. Thermal analysis and microhardness mapping in hybrid laser welds in a structural steel. *Materials Science Forum* 426-432: 4147–4152.
15. Moore, P. L., et al. 2004. Microstructures and properties of laser/arc hybrid welds and autogenous laser welds in pipeline steels. *Science and Technology of Welding and Joining* 9 (4): 314–322.
16. McPherson, N. A., et al. 2005. Laser and laser assisted arc welding processes for DH-36 microalloyed steel ship plate. *Science and Technology of Welding and Joining* 10 (4): 460–467.
17. Stelling, K., et al. 2007. Solidification behaviour and weldability of austenitic steels in laser and hybrid welding. *Welding and Cutting* 6 (3): 27–31.
18. Phillips, E. H., and Metzbower, E. A. 1992. Laser beam welding of HY80 and HY100 steels using hot welding wire addition. *Welding Journal* 71 (6): 201-s to 208-s.
19. Metzbower, E. A., et al. 1994. Microstructures in hot wire laser beam welding of HY 80 Steel. *Materials Science and Technology* 10 (1): 56-59.
20. Lee, T-K., et al. 2000. Effect of inclusion size on the nucleation of acicular ferrite in welds. *ISIJ International* 40 (12): 1260-1268.
21. Liu, S., and Olson, D. L. 1986. The role of inclusions in controlling HSLA steel weld microstructures. *Welding Journal* 65 (6): 139-s to 149-s.
22. Koseki, T., and Thewlis, G. 2005. Inclusion assisted microstructure control in C-Mn and low alloy steel welds. *Materials Science and* Technology 21 (8): 867–879.
23. Osio, A. S., et al. 1996. The effect of solidification on the formation and growth of inclusions in low carbon steel welds. *Materials Science and Engineering* A221: 122–133.
24. Liao, F-C., and Liu, S. 1992. Effect of deoxidation sequence on carbon manganese steel weld metal microstructures. *Welding Journal* 71 (3): 94-s to 103-s.
25. Fox, A. G,. et al. 1996. The effect of small changes in flux basicity on the acicular ferrite content and mechanical properties of submerged arc weld metal of Navy HY-100 steel. *Welding Journal* 75 (10): 330-s to 342-s.
26. Losz, J. M. B., et al. 1995. Microstructural characterization of submerged-arc and gas-metal-arc weldments in HY-130 Steel. *ISIJ International* 35 (1): 71–78.
27. Walpole, Myers, Myers, and Ye. 2002. *Probability and Statistics for Engineers and Scientists.* Upper Saddle River, N.J.: Prentice Hall. P. 165.
28. Hu, B., and den Ouden, G. 2005. Synergetic effects of hybrid laser/arc welding. *Science and Technology of Welding and Joining* 10 (4): 427–431.
29. Nakajima, T. et al. 2002. Radiation phenomena in the groove in laser-arc combination welding. *Welding in the World* 46 (Special Issue): 51–61.